CZECH TECHNICAL UNIVERSITY IN PRAGUE

FACULTY OF MECHANICAL ENGINEERING

DOCTORAL THESIS STATEMENT

ČESKÉ VYSOKÉ UČENÍ TECHNICKÉ V PRAZE

FAKULTA STROJNÍ

ÚSTAV MECHANIKY TEKUTIN A TERMODYNAMIKY

TEZE DISERTAČNÍ PRÁCE

Verified Unsteady Model for Analysis of Contra-Rotating Propeller Aerodynamics

Validovaný nestacionární model pro analýzu aerodynamiky protiběžných vrtulí

Ing. Vít Štorch

Doktorský studijní program: Strojní inženýrství

Studijní obor: Termomechanika a mechanika tekutin

Školitel: prof. Ing. Jiří Nožička, CSc.

Teze disertace k získání akademického titulu "doktor", ve zkratce "Ph.D."

Praha září 2017

Název anglicky:

Verified Unsteady Model for Analysis of Contra-Rotating Propeller Aerodynamics

Disertační práce byla vypracována v prezenční formě doktorského studia na Ústavu mechaniky tekutin a termodynamiky Fakulty strojní ČVUT v Praze.

Disertant: Ing. Vít Štorch
Ústav mechaniky tekutin a termodynamiky, Fakulta strojní ČVUT v Praze, Technická 4, Praha 6, 166 07

Školitel: prof. Ing. Jiří Nožička, CSc.
Ústav mechaniky tekutin a termodynamiky, Fakulta strojní ČVUT v Praze, Technická 4, Praha 6, 166 07

Školitel-specialista: Ing. Jan Čížek, Ph.D.
Ústav mechaniky tekutin a termodynamiky, Fakulta strojní ČVUT v Praze, Technická 4, Praha 6, 166 07

Oponenti:

Teze byly rozeslány dne: .....

Obhajoba disertace se koná dne ..... v …… hod.

v zasedací místnosti č. 17 (v přízemí) Fakulty strojní ČVUT v Praze, Technická 4, Praha 6

před komisí pro obhajobu disertační práce ve studijním oboru Termomechanika a mechanika tekutin.

S disertací je možno se seznámit na oddělení vědy a výzkumu Fakulty strojní ČVUT v Praze, Technická 4, Praha 6.

prof. Ing. Jiří Nožička, CSc.

předseda oborové rady oboru Termomechanika a mechanika tekutin

Fakulta strojní ČVUT v Praze

Verified Unsteady Model for Analysis of Contra-Rotating Propeller Aerodynamics

Resume

The doctoral thesis is focused on the development of a new computational model for analysis of contra-rotating propellers, its testing and verification, and application on selected important problems of contra-rotating propeller aerodynamics. An insight into both past and current state-of-the-art methods for numerical simulation of propellers is provided with focus on contra-rotating propellers. Two of the discussed methods, simpler lifting line method and 3D panel method complemented by boundary layer, are used for rotating blade representation. An unsteady force-free wake model is attached to both blade models for induced velocity determination. Robust 3D panel method is coupled with a two-equation integral boundary layer with a new interaction law that enables seamless solution of boundary layer in regions of strong interaction. As a result, the instantaneous velocity fields, wake shapes, pressure forces and friction forces on the blades are available together with overall performance data for arbitrary contra-rotating propeller geometry. The components of the complex model are tested and validated step by step using well defined problems. The newly developed computational tool is used for analysis of a propeller set and the results are compared with experimental data. Finally, effects of rotational rate ratio, propeller distance, advance ratio and angle of free stream velocity are described and a comparison of contra-rotating propeller to an equivalent single propeller is performed.

Validovaný nestacionární model pro analýzu aerodynamiky protiběžných vrtulí

Abstrakt

Disertační práce je zaměřena na vytvoření nového výpočetního modelu pro analýzu protiběžných vrtulí, jeho ověření a aplikaci na vybrané případy proudění protiběžnými vrtulemi. Práce poskytuje přehled původních a současných metod pro numerické modelování vrtulí se zaměřením na protiběžné vrtule. Dvojice vybraných výpočetních přístupů, metoda nosné čáry a 3D panelová metoda s mezní vrstvou, jsou použity k simulaci listů vrtulí. Nestacionární volný model úplavu je připojen k listům vrtule ztvárněným oběma přístupy, tak, aby bylo možné získat pole indukovaných rychlostí. Osvědčená 3D panelová metoda je spřažena s integrálním dvourovnicovým modelem mezní vrstvy pomocí nového interakčního postupu, který umožňuje bezproblémové řešení rovnic mezní vrstvy v oblastech silné interakce. Výpočetní model umožňuje získávat okamžitá rychlostní pole, tvary úplavů, rozložení tlaku a třecích sil po listech spolu s celkovými výkonnostními parametry pro libovolné tvary vrtulí. Jednotlivé součásti rozsáhlého výpočetního modelu jsou testovány a ověřovány na základě řešení dílčích zjednodušených úloh. Tento nový výpočetní nástroj je posléze použit pro analýzu proudění protiběžnými vrtulemi včetně porovnání s experimentálně získanými výsledky. V závěru práce jsou popsány reakce soustavy protiběžných vrtulí na změnu poměru otáček, vzdálenost rotorů, poměrnou rychlost a úhel nabíhajícího proudění. Rovněž je provedeno porovnání protiběžných vrtulí s odpovídající samostatnou vrtulí.

Contents

Contents i

Abbreviations ii

Symbols iii

1 Introduction 1

2 Propeller Aerodynamics 2
- 2.1 Propeller performance . . . 2
- 2.2 Current state of propeller research by various methods . . . 2

3 Potential Flow Theory and Related Methods 5
- 3.1 Potential flow . . . 5
  - 3.1.1 Boundary conditions . . . 5
- 3.2 Panel methods . . . 5

4 Formulation of Aims and Objectives 7

5 Vortex Wake Model 8
- 5.1 Vortex filament in 3D space . . . 8
- 5.2 Vortex filament growth and stretching . . . 8
- 5.3 Unsteady 3D vortex wake model . . . 9

6 Propeller Blade Representation 10
- 6.1 Lifting line model . . . 10
- 6.2 Model based on 3D panel method . . . 11

7 Coupled 2D Integral Boundary Layer Model 13
- 7.1 Boundary layer viscous-inviscid coupling . . . 14
- 7.2 Portable boundary layer model . . . 15
- 7.3 Replacement inviscid model . . . 15

8 Experimental Investigation of Contra-Rotating Propellers 17

9 Results, Analysis and Discussion 18
- 9.1 Verification of the models . . . 18
- 9.2 Results of numerical analysis of CRP . . . 19

10 Conclusions and Recommendations 21
- 10.1 Contribution in the field of computational methods . . . 21
- 10.2 Contribution in the field of propeller aerodynamics . . . 21
- 10.3 Recommendations on the future work . . . 22

References 23

Cited and uncited work of the author 26

Abbreviations

BEM	**B**lade **E**lement **M**omentum
BL	**B**oundary **L**ayer
CFD	**C**omputational **F**luid **D**ynamics
CRP	**C**ontra-**R**otating **P**ropeller
LL	**L**ifting **L**ine (method)
LS	**L**ifting **S**urface (method)
NACA	**N**ational **A**dvisory **C**ommittee for **A**eronautics
PM	**P**anel **M**ethod
PWM	**P**ulse **W**idth **M**odulation
RANS	**R**eynolds **A**veraged **N**avier **S**tokes
UAV	**U**nmanned **A**erial **V**ehicle
VAWT	**V**ertical **A**xis **W**ind **T**urbine

Symbols

A	area	m^2
b	chord length	m
c	velocity	m s^{-1}
c_∞	free stream velocity	m s^{-1}
C_D	boundary layer dissipation coefficient	1
C_f	skin friction coefficient	1
C_τ	shear stress coefficient	1
$C_{\tau EQ}$	equilibrium shear stress coefficient	1
c_P	power coefficient	1
c_T	thrust coefficient	1
c_Q	torque coefficient	1
D	diameter	m
d_{ij}	interaction coefficient	s^{-1}
FoM	Figure of Merit	1
f	frequency	Hz
H	boundary layer shape parameter	1
H^*	kinetic energy shape parameter	1
$\vec{n}$	normal vector	m
$\tilde{n}$	Tollmien-Schlichting wave amplif. exponent	1
P	power	W
p	pressure (static)	Pa
R	radius	m
r	radial coordinate	m
$\vec{r}$	radius vector	m
Re	Reynolds number	1
T	thrust force	N
t	time	s
u_e	boundary layer edge velocity	m s^{-1}
x, y, z	global coordinates	m
Γ	circulation	$m^2 s^{-1}$
δ^*	displacement thickness	m
δ_{99}	boundary layer thickness by convention	m
η	efficiency	1
θ	momentum thickness	m
λ	propeller advance ratio	1
ξ	streamwise BL coordinate	m
ν	kinematic viscosity	$m^2 s^{-1}$
ρ	density	kg m^-3
ϕ	potential	$m^2 s^{-1}$

1. Introduction

A contra-rotating propeller system consists of a pair of propellers sharing the axis of rotation and rotating in the opposite direction. The propellers interact producing a very complex problem of rotor aerodynamics.

The benefits of contra-rotating propellers (CRPs) could be summarized as: 1) high efficiency under high loads, 2) low reaction torque, 3) high maximum thrust power for a given diameter. Drawbacks of CRP systems which limit their wider spread include higher mechanical complexity, high noise levels, complex aerodynamic design and often lower efficiency when used improperly.

The ultimate decision whether to use a CRP system or not depends on the exact problem definition, design limits and operating conditions of the device. In the growing field of UAV propulsion, vehicles of all sizes and purposes are in need of carefully tailored mission-specific propulsion systems. Especially small scale propellers operating in low Reynolds number flows were long time overlooked due to limited industrial application in the past. Research of the aerodynamic properties of CRP systems and development of an experimentally verified and robust computational tool is therefore highly desirable.

The doctoral thesis is focused on gathering available information and data on the topic of contra-rotating propellers, building a suitable numerical model, step by step, and describing the aerodynamics of CRPs using the newly developed numerical model and own experimental results. Last but not least, the goal is to extend the available numerical methods for analysis of lifting bodies to enhance their capabilities.

There are two branches of computational methods currently used for propeller (less frequently CRP) analysis. Both have their advantages and disadvantages. In terms of complexity and depth of modeled phenomena, Navier-Stokes equation solvers are the most complex and resource demending. Time-stepping solution with sliding mesh techniques operating on fine meshes requires large computer clusters and significant amount of time. For this reason, second branch of computational methods is often used which includes simpler solvers derived from blade element momentum methods or methods based on potential flow theory. Such methods are much more suitable for general analysis of CRP systems due to faster solution (by several orders of magnitude) and are covered in the thesis. A 3D panel method and a boundary layer model were chosen as the basic ingredients of the novel computational model presented in the thesis.

2. Propeller Aerodynamics

2.1 Propeller performance

The operational conditions are defined by density ρ, free stream velocity c_∞, propeller angular velocity $\Omega = 2\pi f$ and angle of the free stream relative to rotation axis φ.

To better evaluate performance of propellers, non-dimensional values of advance ratio λ, thrust coefficient c_T, torque coefficient c_Q, power coefficient c_P and efficiency η are used. Standard definitions of these parameters for single propellers can be found for example in [1]. For a CRP system the following definitions of dimensionless parameters are used (index 1 indicates properties of upstream propeller, index 2 indicates properties of downstream propeller):

$$c_T = \frac{T_1 + T_2}{\rho 0.25(f_1^2 + f_2^2)(D_1^4 + D_2^4)}. \tag{2.1}$$

$$c_Q = \frac{Q_1 + Q_2}{\rho 0.25(f_1^2 + f_2^2)(D_1^5 + D_2^5)}. \tag{2.2}$$

$$c_P = \frac{P_1 + P_2}{\rho 0.25(f_1^3 + f_2^3)(D_1^5 + D_2^5)}. \tag{2.3}$$

$$\tag{2.4}$$

To evaluate the efficiency of propellers producing thrust in static regime, term Figure of Merit or "static efficiency" FoM is used. The Figure of Merit definition for CRP systems is discussed in detail by Leishman and Ananthan in [2]. The following definition of FoM for CRP is used for the purpose of this work:

$$FoM = \frac{(T_1 + T_2)^{3/2}}{(P_1 + P_2)\sqrt{2\rho\, max(A_1, A_2)}}. \tag{2.5}$$

Swirl losses are an important factor when CRP propellers are discussed because the downstream propeller can reduce or almost eliminate wake swirl which leads to increased efficiency. The power lost due to swirl losses can be derived from the kinetic energy of the rotating wake and is calculated according to Eq. (2.6).

$$P_{swirl} = \frac{1}{2}\rho \int 2\pi r c_a {c_\theta}^2 dr. \tag{2.6}$$

Propeller Reynolds number is based on the blade chord b at characteristic radius $r/R = 0.75$ and local relative velocity c_{rel}:

$$Re = \frac{c_{rel} b}{\nu}. \tag{2.7}$$

2.2 Current state of propeller research by various methods

Simplest methods based on momentum theory replace propeller by an actuator disc with constant pressure jump across its surface. In case of a CRP system, two actuator discs are used (see

Figs. 2.1 and 2.2). The momentum approach alone is not sufficient to investigate real propellers with general geometries. The blade element approach divides the blades into several elements and lift and drag are investigated at each blade section. This approach only works when induced velocity is correctly accounted for. Combining these two approaches, blade element momentum (BEM) method uses momentum equations to calculate induced velocity at blade sections. It is a rather simple method used regularly for optimization and quick design and analysis purposes. BEM is used in an analysis of contra-rotating propellers by Leishman and Ananthan [2]. A similar approach is used by Rand and Khromov [3] to find an optimum rotor design for hover and axial flight using lookup tables for lift and drag.

More accurate induced velocity distribution is obtained by using vortex filament wake model attached to a system of bound vortices oriented along blade span. This approach is described in the thesis as lifting line (LL) model, although in some literature it is classified as a variant of vortex lattice model. Lifting surface (LS) model represents blades by a surface of vortex panels which respects the actual blade width, but not its thickness. It is used frequently for analysis of marine propellers due to their low aspect ratio. Yang et al. [4] used lifting surface in their early work (1992) on contra-rotating ship propellers. The wake is modeled using relaxation method, where the averaged induced velocity of both propellers is used to define the pitch of the trailing wake system.

Full blade geometry representation is achieved by using 3D panel method. 3D panel method was first applied on the case of propellers by Hess and Valarezo [5]. Extension for calculating unsteady forces was done by Hsin [6] in his work aimed at single marine propellers. Ghassemi [7] describes software package SPD (Ship Propeller Design) that uses panel method with hyperboloidal quadrilateral elements to model CRP. The method calculates thrusts and torques without including viscous forces. Between 2 and 3 percent of increase in efficiency was obtained using the CRP system for the studied CRP case compared to single propeller.

The impact of using a proper boundary layer model instead of some viscous corrections for single propeller analysis is described by Takinaci and Atlar [8]. The authors use turbulent model of Cebeci and Bradshaw without any coupling between boundary layer and inviscid flow.

Advanced CFD codes (here used as a synonym for Navier-Stokes equation solvers) have been used in some studies regarding single and contra-rotating propellers. CFD codes have seen only limited use in the analysis or even optimization of propellers, although the trends towards using these CFD codes are more and more evident. Especially in case of single rotor, which can be often computed using steady solvers, the solution time becomes manageable. Reynolds-Averaged Navier Stokes (RANS) solver is the most widely used approach for CFD analysis of propellers.

An interesting comparison of results calculated by CFD code and 3D panel method for a case of single ship propellers is that of Brizzolara et al. [9]. Both methods agree well with the experimental data, except of some small regions of the blades, where the boundary layer thickness affects the pressure field and RANS solver provides more accurate results. The authors suggest that the panel method should be coupled with boundary layer model. Other notable studies of CRP systems using CFD codes include [10] and [11]. A very recent (2015) paper by Paik et al. [12] compares the results of wake development behind ship CRP setup calculated by

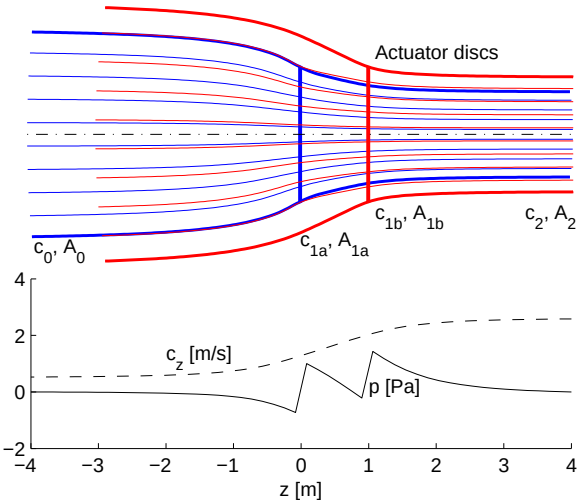

FIGURE 2.1: CRP Actuator disc streamtubes, non-zero free stream velocity.

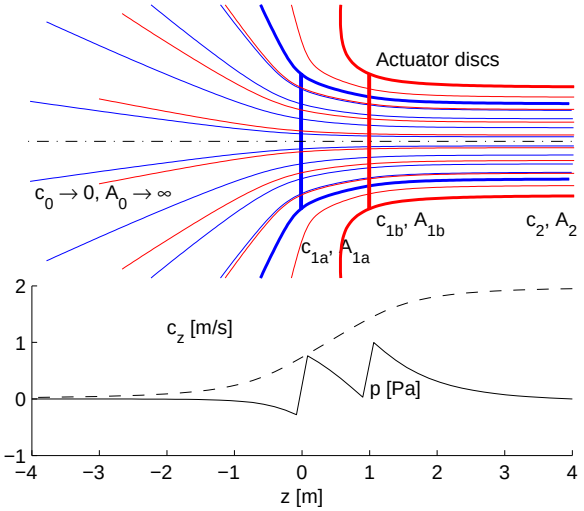

FIGURE 2.2: CRP Actuator disc streamtubes, zero free stream velocity.

CFD RANS unsteady solver and results of Stereo PIV measurement. The study focuses mainly on the position and development of blade tip vortices and illustrates the complexity of using CFD for CRP analysis.

Experimental research, in a similar way as numerical research, is more frequently focused on marine propellers. In the field of airspace CRP usage most work concerns helicopter rotors. Full scale tunnel test as early as 1951 were performed in Langley [13]. The results of hovering performance were compared with numerical methods of that time. The maximum FoM for a coaxial rotor was determined to be 0.635 while for single rotor it was 0.615. Three years later, a similar research [14], which included also visualization, confirms improved hovering efficiency of a CRP system, but notes that more power is required for level flight than in case of equivalent single rotor. Comprehensive overview of coaxial rotor helicopter experimental research, mostly by the helicopter manufacturers, is given in [15].

A different configuration, with motors and support structure placed between the rotors, is presented in an article by Huo et al. [16]. The rotor was equipped with a long shroud. The performance of both rotors and the shroud were measured individually. Similar experimental setup as of Huo et al. but without shroud is used by Simoes [17] who measured performance of a coaxial system with 14x4.7 propellers. His results are in disagreement with outcomes of others, since he determined that two propellers rotating in the same direction were a better option than CRP system.

An experimental study about hover performance of single, tandem and coaxial rotors [18] shows a very viable solution of the measurement setup. This paper among others lists the parameters of other previous experiments on this topic. The measurement confirmed, that overall performance is not very sensitive to propeller distance, but the load distribution between rotors changes with propeller distance. CRP system was found to have a 9% higher FoM than an equivalent single propeller.

3. Potential Flow Theory and Related Methods

3.1 Potential flow

Potential flow is an inviscid irrotational flow which can be expressed by Laplace's equation:

$$\nabla^2\phi = \Delta\phi = \frac{\partial^2\phi}{\partial x^2} + \frac{\partial^2\phi}{\partial y^2} + \frac{\partial^2\phi}{\partial z^2} = 0, . \tag{3.1}$$

where ϕ is a velocity potential, which is a function of space and time. Laplace's equation is an elliptic partial differential equation. Solutions to the Laplace's equation are called harmonic functions. Laplace's equation does not contain a pressure term. To obtain information about pressure, it is necessary to use the Bernoulli's equation in the form for incompressible irrotational flow with conservative forces [19]:

$$gz + \frac{p}{\rho} + \frac{c^2}{2} + \frac{\partial\phi}{\partial t} = C(t), \tag{3.2}$$

where z is a coordinate in opposite direction to gravitational acceleration and $C(t)$ is a constant only changing with time.

3.1.1 Boundary conditions

Boundary condition must be specified at the surface of the body and in the infinity. In the infinity the assumption of vanished induced velocity due to presence of the body must be valid, therefore the total velocity in sufficient distance from the body is equal to the free stream velocity:

$$\lim_{r\to\infty} c = c_\infty. \tag{3.3}$$

This condition is in most cases fulfilled automatically by superposition of suitable singular solutions of Laplace's equation. Impermeability condition is applied on the surface of the body. In every moment the velocity vector on the surface of the body, expressed in the coordinate system fixed to the body, must be tangent to the surface, or zero. This condition is equivalent to the requirement of zero normal velocity on the surface. It is a Neumann type of boundary condition:

$$\frac{\partial\phi}{\partial n} = \nabla\phi \cdot \vec{n} = 0. \tag{3.4}$$

There are several methods for solving Laplace's equation. Since Laplace's equation is linear, it is possible to use a linear combination of simple solutions. The most common solutions are the potential vortex, potential source/sink and dipole (doublet). 2D and 3D panel methods use this approach.

3.2 Panel methods

Panel methods use line segments or curve segments with concentrated or distributed singular solutions, such as vortex or source. In 2D, panels are represented by line segments or curve

segments, while in case of 3D panel methods, panels are formed by flat or curved polygons, most frequently quadrilaterals. A simple 2D panel method which uses streamfunction formulation [20] is used in the thesis only for verification of 2D boundary layer. Focus is therefore on 3D panel methods, which form a cornerstone of the described computational model.

There are two branches of 3D panel methods based on type of boundary conditions. Zero velocity normal to the wall is prescribed by Hess type panel methods, first described by Hess and Smith [21], and Hess [22]. These panel methods use velocity formulation of simple singular solutions. In 1974 a very different formulation of panel method has been published by Morino and Kuo [23]. The family of methods, later named after Morino, use a potential formulation and a different form of boundary condition, which prescribes zero potential inside the body. A detailed review of various boundary conditions is available by Erickson [24].

High order panel methods use quadratic and cubic definitions of the panel surface, but more common are low order panel methods that use either quadrilateral or triangular flat panels. As Smith and Hess note [21], a quadrilateral surface mesh can be easily made structured, on the other hand with triangular elements it is possible to cover a complex body without gap

In order to calculate lifting flow, Kutta condition for the trailing edge must be implemented. According to Kelvin's circulation conservation law the bound vortex circulation cannot end in the fluid and zero trailing edge circulation must be forced. To lead the circulation away from the wing a system of trailing vortices is shed from the trailing edge. This is in practice performed by either a sheet of semi-infinite vortices connected to the trailing edge, or by a force-free wake sheet composed of vortex ring panels. Either way, the circulation of the wake vortices is calculated as the difference between upper and lower trailing edge panel circulation.

4. Formulation of Aims and Objectives

The aim of this thesis is to develop a computational model capable of detailed analysis of contra-rotating propellers subject to low Reynolds number flow accounting for various aspect of the flow ignored by other researchers. The aim is also to describe the properties of contra-rotating propellers using such advanced computational model and answer important questions regarding CRP system performance. The formulation of three main objectives is based on the review of literature and is given as follows:

- Finding a viscous-inviscid interaction model that would allow coupling of an advanced integral boundary model to a 3D panel method. This model must be fast enough to maintain the important advantage over CFD codes - speed of solution.
- Creating an unsteady force-free wake model compatible with contra-rotating propeller configuration with emphasis on blade-wake interactions, which would allow accurate resolving of instantaneous wake shapes and induced velocity fields.
- Describing properties of a contra-rotating propeller system under low Reynolds number flow regimes, specifically:
  - Fluctuation of forces and torques during revolution
  - Influence of propeller distance
  - Sensitivity to the angle of free stream flow
  - Comparison of a CRP system to an equivalent single propeller
  - Influence of the ratio of rotational speeds of both propellers

Secondary goals and steps that need to be taken in order to accomplish the objectives include: (1) selecting suitable boundary layer model for implementation, (2) design of experimental setup and performing measurements of CRP properties including noise, (3) preparing simpler lifting line model for reference purposes and (4) verification of numerical model using experimental data.

5. Vortex Wake Model

Vortex wake model consists of quadrilateral vortex ring panels that are shed from the trailing edge of a blade or directly from the lifting line representing the blade. Each vortex ring panel is formed by four vortex filaments placed at the edges.

5.1 Vortex filament in 3D space

Vortex filament is a line vortex between starting (1) and ending (2) points. The following formula is used for determining velocity at a point P in space.

$$\vec{c} = \frac{\Gamma}{4\pi} \frac{\vec{r}_1 \times \vec{r}_2}{|\vec{r}_1 \times \vec{r}_2|^2} \vec{r}_0 \cdot \left(\frac{\vec{r}_1}{|\vec{r}_1|} - \frac{\vec{r}_2}{|\vec{r}_2|} \right). \tag{5.1}$$

The vector leading from point 1 to P is defined as $\vec{r}_1$, the vector from point 2 to point P is $\vec{r}_2$ and the vector from first to second point of the vortex segment is defined as $\vec{r}_0$.

In order to overcome difficulties with singular solution and unphysical velocities near vortex filament, several core models were tested. Based on review of literature and evaluating performance of calculation of Rankine, Lamb-Oseen [25], Burnham-Hallock [26] and Vatistas [27] core models, Lamb-Oseen core model was chosen for implementation in the vortex wake.

The Lamb-Oseen vortex core model has been extended to a 3D filament case in [A 1] by the author. Core radius is denoted as R_C:

$$\vec{c} = \frac{\Gamma}{4\pi} \frac{\vec{r}_1 \times \vec{r}_2}{|\vec{r}_1 \times \vec{r}_2|^2} \vec{r}_0 \cdot \left(\frac{\vec{r}_1}{|\vec{r}_1|} - \frac{\vec{r}_2}{|\vec{r}_2|} \right) \left[1 - exp\left(-1.2526 \frac{|\vec{r}_1 \times \vec{r}_2|^2}{R_C^2 |\vec{r}_0|^2} \right) \right]. \tag{5.2}$$

The model of vortex filament has been tested using self-induced velocity of circular vortex rings. The testing revealed that larger core results in slower self-induced velocity and higher number of segments is required for properly capturing self-induced velocity in case of a thin core. A study by Batchelor [28] confirms that a curved vortex filament without viscous core moves with infinite speed under the action of the self-induced velocity field.

5.2 Vortex filament growth and stretching

In case of non-zero initial vortex core size R_{Ci} the core growth is calculated as follows [29]:

$$R_C = \sqrt{R_{Ci}^2 + 4\nu t}. \tag{5.3}$$

Free vortex filaments in a general velocity field can either decrease or more likely increase their length. The influence of the vortex stretching on the rotor dynamics results is discussed in [30], together with the explanation of the process of stretching, which can be simulated by decrease in the viscous core size while maintaining constant circulation. The change of core radius ΔR_C due to strain $\epsilon = (l + \Delta l)/l$ is expressed as follows [30]:

$$\Delta R_C = R_C \left(1 - \frac{1}{\sqrt{1+\epsilon}} \right). \tag{5.4}$$

5.3 Unsteady 3D vortex wake model

Regardless of the wing representation type (LL, LS or 3D panel method), the wing model provides a bound circulation distribution, which needs to be shed into the wake.

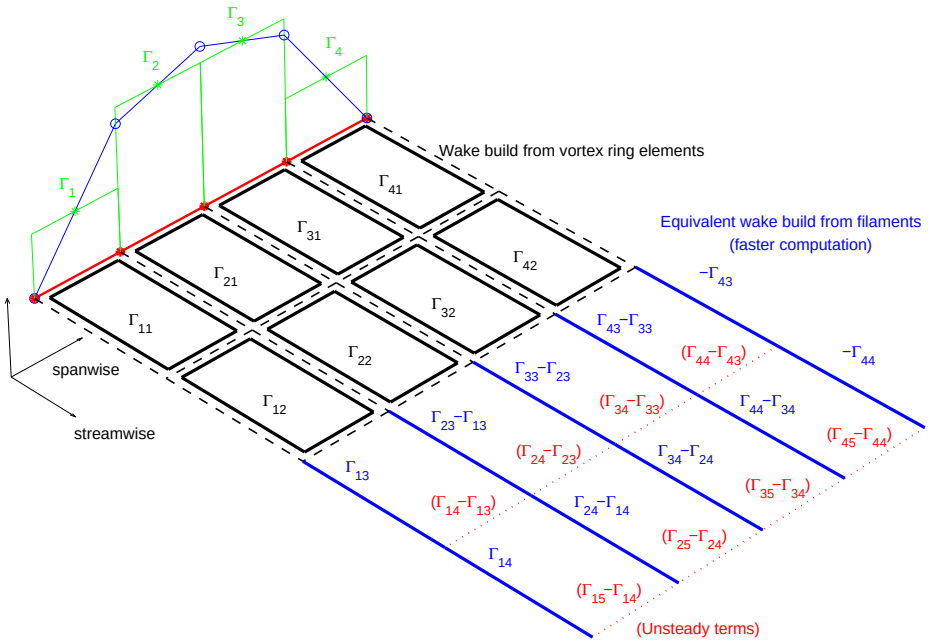

FIGURE 5.1: Vortex wake structure and nomenclature. Both vortex filament and vortex ring approaches are shown.

Vortex lattice wake model (see Fig. 5.1) is composed of rectangular vortex ring segments. At each time step the existing wake panels are convected downstream using the local velocity value. A new vortex panel per spanwise station i is shed, with circulation Γ_{i1}. The original vortex panels being convected downstream increase their row number by one $\Gamma_{i,j} = \Gamma_{i,j+1}$. Neighboring edges of panels produce duplicate filaments, only with different circulation values. Almost twofold reduction in computation time is obtained by combining neighboring panel edges into single filament.

This concept of an unsteady wake was tested by the author et al. in an investigation of vertical axis wind turbines both numerically and experimentally [A 2].

6. Propeller Blade Representation

6.1 Lifting line model

Lifting line model is used in the thesis as an alternative to the complex computational model composed of 3D panel method with boundary layer. It can use the same vortex wake model, which is beneficial for testing purposes and for fair comparison of the two blade representations. Lifting line approach is based on simplified finite wing representation described by Prandtl's lifting line theory. For a symmetric wing with frozen (predefined) flat wake and small angles of attack the analytic solution of Glauert can be used, which is however not possible for the case of propeller blades. Numerical solution using iterative process needs to be used.

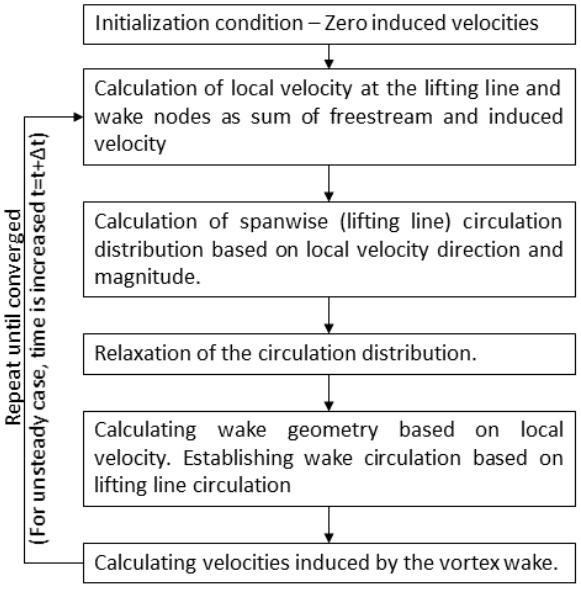

FIGURE 6.1: Block diagram of the iterative solution procedure.

The solution procedure (see Fig. 6.1) is iterative and begins with lifting line with no wake and thus no induced velocities. Under-relaxation is usually required to keep the solution stable. The simplest method of discretization consists of averaging the circulation distribution over a lifting line segment, which produces a piecewise constant distribution of circulation that can be directly used in the wake model. This approach leads to an issue with erratic induced velocity distribution at the blade tips. This issue was solved, as documented in the thesis, by modifying the position of the tip vortex shedding station without altering the positions of points where induced velocity is evaluated.

Lift, induced drag and viscous drag are computed from 2D airfoil polars pre-computed in XFOIL and induced velocity vectors. The algorithms are verified using a case of rectangular wing set to a sudden motion and the same wing performing oscillating motion.

6.2 Model based on 3D panel method

Velocity formulation (Hess type) panel method was chosen for implementation with the boundary layer model. It is described in detail in [A 3]. Two types of singularity distributions over the panels are used: vortex ring panels and constant source distribution. Quadrilateral panels form a structured surface mesh. Each blade is unwrapped into a 2D mesh, which is consistent with 2D matrices that store the geometry data. Matrix rows represent the data in the streamwise direction and matrix columns represent the data in the spanwise direction. (see Fig. 6.2)

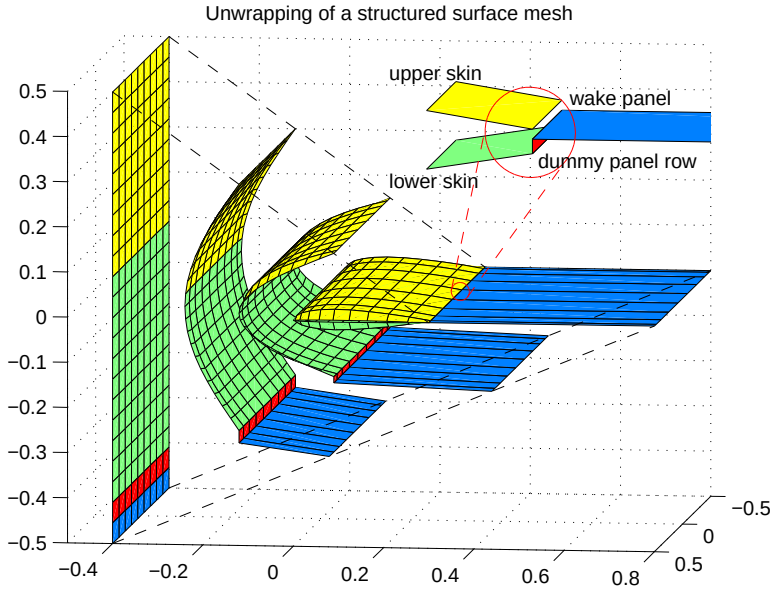

FIGURE 6.2: Structured surface mesh of a wing (applies also to a propeller blade).

The dummy panel row visible in the figure is a helper object which solves the problem with finite edge thickness, where the lower T.E. panel coordinates do not coincide with wake panel coordinates. For an unsteady case of a finite wing or for rotating blades the first wake panel row is rather short and is connected to the wake model described in Chapter 5.

A simplified block diagram of the unsteady solution process is in Fig. 6.3. Each blade is initialized in its starting position, together with a single row of wake panels. The body rotation is handled by a standalone function, which first rotates the body by specified angles around x, y, z axes. When the body is rotated into new position, the local relative velocity due to this rotation is calculated. The principle of wake convection can be seen in Fig. 6.4. The wake nodes are convected in the direction of total velocity at each node, calculated as the sum of free-stream, self-induced and body-induced velocities calculated in previous iteration. The algorithms are tested on cases of rectangular wing performing sudden start and oscillating motion.

Several issues had to be solved in order to apply the computational model to contra-rotating propellers. Propeller geometry was modified to remove problematic root section with blunt trailing edge. A procedure named “wake blow off” helps to solve the issue of low advance ratio wake development as illustrated in Figs. 6.5 and 6.6 .

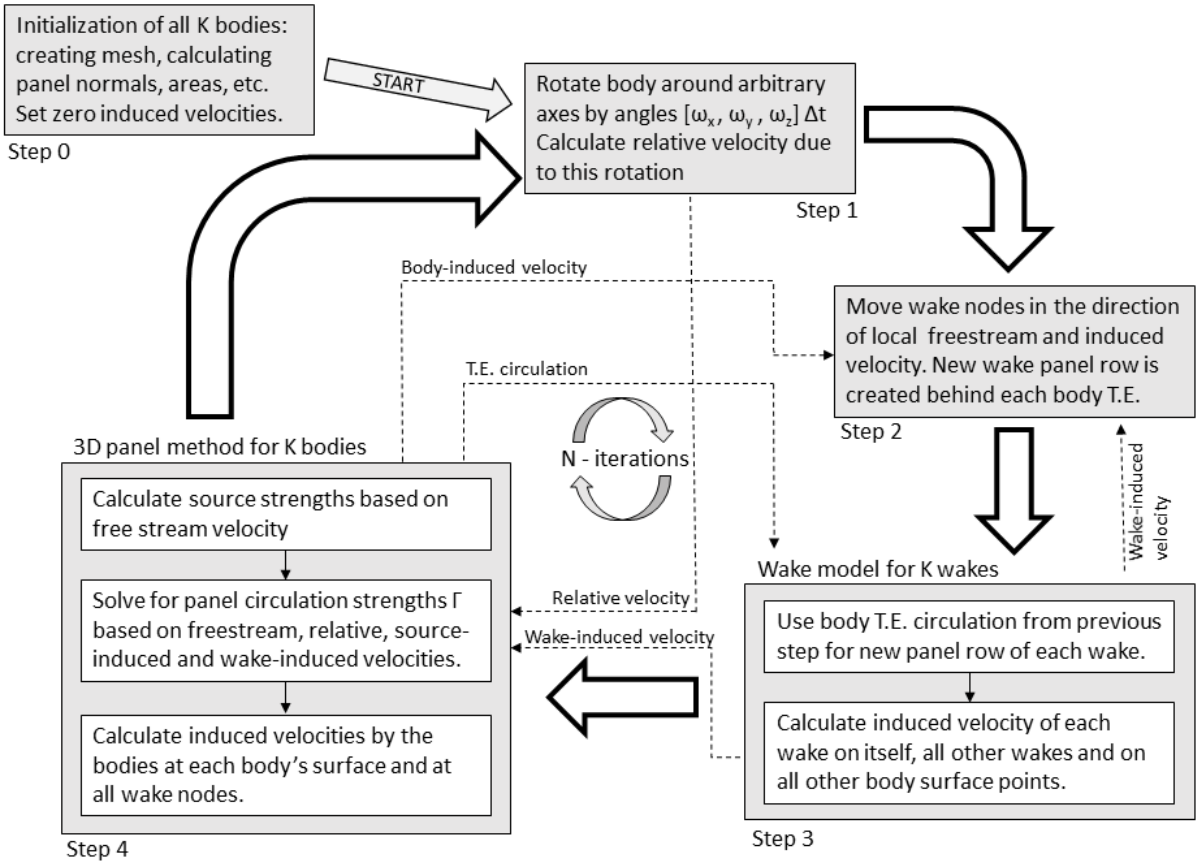

FIGURE 6.3: Simplified block diagram of the unsteady solver.

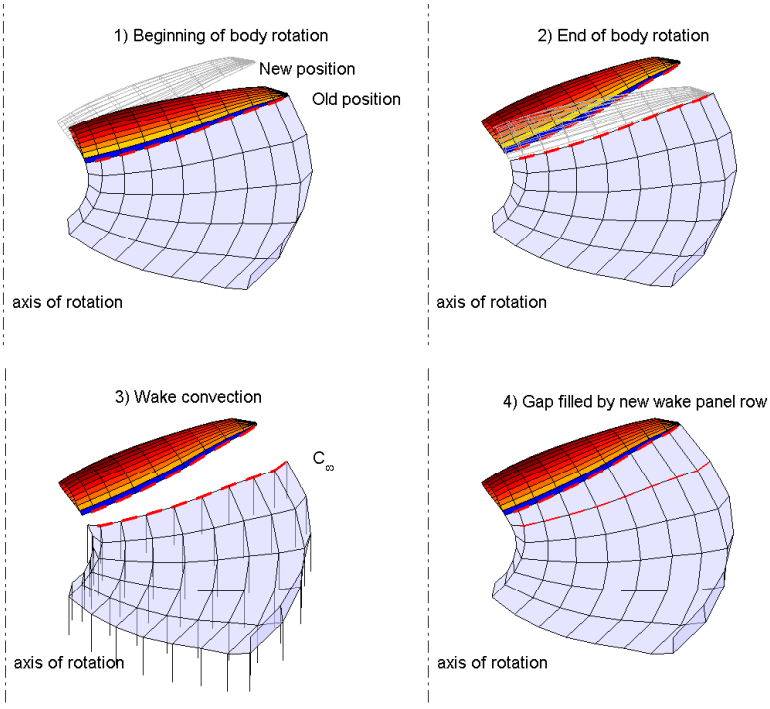

FIGURE 6.4: Body to wake linkage has 4 phases.

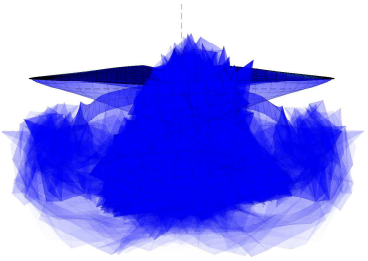

FIGURE 6.5: Wake behind propeller, without wake blow off.

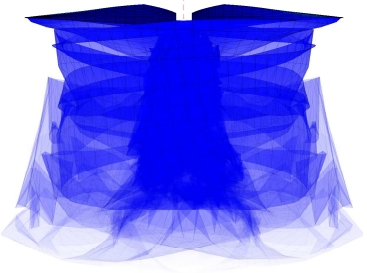

FIGURE 6.6: Wake behind propeller, with wake blow off.

7. Coupled 2D Integral Boundary Layer Model

The integral two-equation 2D boundary layer model used in this work is based on the work of Drela [20] and Drela and Giles [31], Johansen [32], Green et al. [33], Veldman [34] and Bijleveld and Veldman [35]. Detailed description of the model together with results of airfoil analysis can be found in [A 4].

The fluid domain is divided into viscous region and inviscid region. Goal of the viscous-inviscid interaction model is to link (couple) the inviscid solver with boundary layer solver.

Key component of the integral boundary layer is a velocity profile, which is parametrized by the boundary layer properties. The first governing equation of the integral boundary layer model is the integral momentum equation:

$$\frac{d\theta}{d\xi} + (2+H)\frac{\theta}{u_e}\frac{du_e}{d\xi} = \frac{C_f}{2}. \tag{7.1}$$

The second governing equation of the described boundary layer model is the kinetic energy shape parameter equation

$$\theta\frac{dH^*}{d\xi} + H^*(1-H)\frac{\theta}{u_e}\frac{du_e}{d\xi} = 2C_D - H^*\frac{C_f}{2}. \tag{7.2}$$

The primary variables were chosen H and θ. The edge velocity u_e depends on the boundary layer displacement thickness and inviscid solution and is treated as a function of primary variables $u_e = u_e(H,\theta)$. The remaining parameters of the boundary layer equation are all functions of the primary variables $H^* = H^*(H,\theta)$, $C_f = C_f(H,\theta)$ and $C_D = C_D(H,\theta)$. These functions are provided in form of closure equations [20]. An auxiliary equation is solved together with the governing equations, which is different for turbulent and for laminar regions.

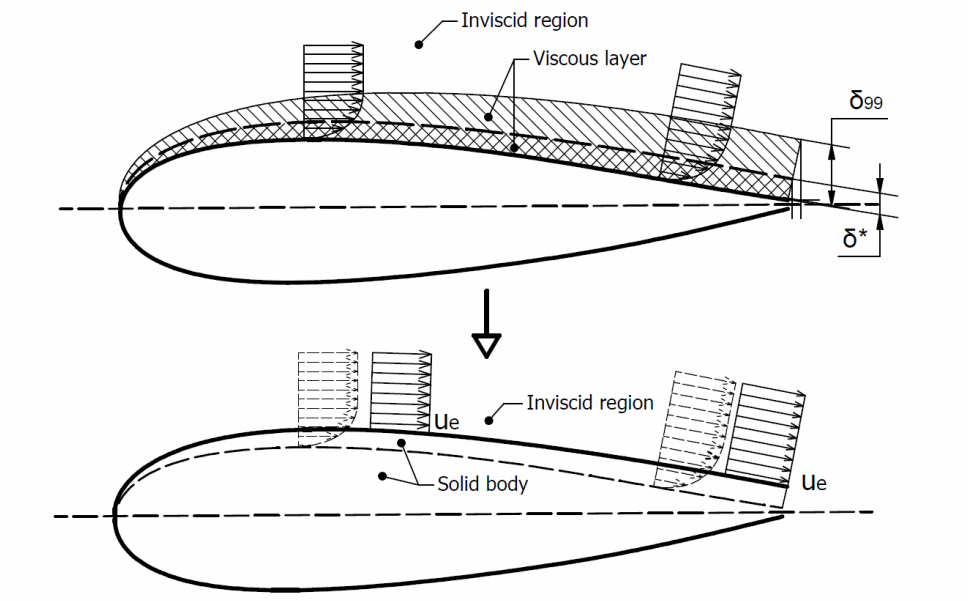

FIGURE 7.1: Solution of the boundary layer problem using viscous and inviscid regions (Figure also used in [A 4]).

For transition prediction, the e^9 method also used in the XFOIL [20] and ISES code [31] is employed. The equation for amplification ratio is solved together with governing equations in laminar region. When the value of amplification ratio reaches the predefined critical value $\tilde{n}_{crit}$ the transition occurs and solution switches to turbulent closure equations.

An auxiliary equation for shear stress coefficient is calculated in the turbulent region. Green et al. [33] proposed a lag-entrainment method which calculates C_τ based on its equilibrium value $C_{\tau EQ}$ and its spatial rate of change.

To solve the boundary layer equations, a simple downstream marching algorithm is used. The governing equations are discretized using two-point central differencing scheme and solved by Newton iteration method, station after station, during downstream pass of the boundary layer.

7.1 Boundary layer viscous-inviscid coupling

The described two equation boundary layer model fails to produce solution in most circumstances if a prescribed edge velocity distribution is used. This is due to a singular behavior of the governing equations described by Goldstein for conditions near separation [36]. To obtain converged solution, interaction between boundary layer and inviscid solution must be provided in form of a relation between edge velocity and displacement thickness.

A two dimensional airfoil analysis tool XFOIL by M. Drela [20] uses simultaneous solutions of boundary layer equations and 2D panel method equations in one large system. Extending this approach to a three-dimensional body is associated with many difficulties.

The boundary layer coupling implemented in present model uses different, quasi-simultaneous, solution approach. This topic is covered by Veldman [34], who discussed the criteria for convergence and existence of the solution and described a simple interaction law [37].

The first step that was performed in search of a suitable viscous - inviscid interaction model was an exact determination of linear coefficients d_{ij} describing change of edge velocity at i-th node due to change of displacement thickness at j-th node:

$$d_{ij} = \frac{\partial u_{e\,i}}{\partial \delta^*_j}. \tag{7.3}$$

These linear coefficients form a response matrix, which can be used for precise determination of new velocity distribution, when the shape of the airfoil changes (with assumption of small displacements of the airfoil surface). An example of such response matrix is presented in Fig.7.2. Important feature of the matrix is a dominating positive main diagonal with still significant negative subdiagonal and superdiagonal. Other members of the matrix have less significant values. Each coefficient on the main diagonal d_{ii} shows the response of edge velocity at i-th surface node to its own displacement in normal direction. Therefore the coefficients from main diagonal can be used in an interaction law:

$$u_{e\,i,NEW} = u_{e\,i,OLD} + d_{ii}(\delta^*_{i,NEW} - \delta^*_{i,OLD}). \tag{7.4}$$

d_{ij}	j=1	2	3	...	...	...	...	...	...	...	...	...	...	...	...	...	...	N
i=1	8.9	−5.2	−1.3	−1.4	−1.3	−1.5	−1.9	−3.1	−6.3	2.8	1.6	1.1	0.9	0.7	0.7	−0.7	8.9
2	−3.1	12	−3.9	1	0.8	1.2	1.7	3.1	6.7	−3.2	−1.9	−1.4	−1.1	−1.1	−1.3	0.2	−3.1
3	−0.2	−5.2	12.1	−5.7	0	−0.4	−0.2	−0.2	−0.1	0	0	0	−0.1	−0.2	0.6	−0.4	−0.2
...	−0.1	0.2	−5.8	14.2	−6.9	0	−0.5	−0.2	0.1	−0.2	−0.1	−0.2	−0.2	0.4	−0.3	−0.3	−0.1
...	0	−0.3	0.3	−7.2	17.6	−9.3	−0.3	−1	−0.8	0.1	−0.1	−0.1	0.4	−0.2	−0.2	0	0
...	0	−0.1	−0.4	0.5	−9.3	23.5	−13.	−1.1	−2.1	0.1	0	0.5	−0.1	−0.2	0	0	0
...	0	−0.1	−0.1	−0.5	0.8	−13.	35	−26	−3.1	0.6	0.9	0	−0.1	0.1	0	0	0
...	0	0	−0.1	−0.1	−0.8	1.6	−21.	53.1	−49.	−1.6	1.1	−0.1	0.2	0	0	0	0
...	0	0	0	−0.1	−0.1	−0.8	2.1	−23.	16.5	12.6	−0.8	0.5	0.1	0.1	0	0	0
...	0	0	0	0	0	0	−0.2	0.4	5.6	14	−5.8	0.4	−0.2	0	0	0	0
...	0	0	0	0	−0.1	−0.1	0.4	0.5	1.8	−13.	19.2	−7.5	0.4	−0.3	−0.1	0	0
...	0	0	0	−0.1	−0.1	0.3	0.1	0.1	1.4	−0.7	−9.5	16.2	−6.5	0.3	−0.3	−0.1	0
...	0	0	−0.1	−0.2	0.3	−0.1	−0.1	0.1	0.6	−0.8	−0.2	−7.2	13.6	−5.6	0.2	−0.2	0
...	−0.1	−0.2	−0.3	0.3	−0.2	−0.2	−0.1	−0.1	−0.1	−0.1	−0.4	0	−5.8	11.8	−4.9	0.1	−0.1
...	−0.1	−0.4	0.6	−0.2	−0.1	0	0	0	0.1	−0.2	−0.2	−0.4	0	−5	10.6	−4.6	−0.1
...	−3	0.1	−1.2	−1	−1	−1.3	−1.7	−2.9	−6.2	2.8	1.6	1.1	0.7	0.9	−3.6	11.1	−3
N	9	−0.6	0.7	0.7	0.9	1.1	1.6	2.8	6.3	−3.1	−1.9	−1.5	−1.3	−1.4	−1.3	−5.2	9

FIGURE 7.2: Typical matrix of velocity response to displacement thickness

Numerical differentiation was initially tested for calculating linearized interaction coefficient d_{ii}. This method is computationally expensive, therefore a fast way of approximating the interaction coefficient d_{ii} based on only one inviscid solution was invented:

$$d_{ii} = \frac{2u_{e\,i,inv}}{(\xi_i - \xi_{i-1})}. \tag{7.5}$$

7.2 Portable boundary layer model

The local linear interaction coefficient d_{ii} only estimates the local response of edge velocity to a local change of displacement thickness. Further boundary layer passes, with inviscid flow solution updates in-between, are necessary to arrive at a converged solution. Even with an accurate linear interaction coefficient, between 10 and 20 passes are required for converged solution. This is a known problem of quasi-simultaneous viscous-inviscid interaction methods [37].

To make the boundary layer model easily portable, a replacement inviscid model is proposed, which allows to approximate the edge velocity based on initial surface velocity distribution and displacement thickness alone.

7.3 Replacement inviscid model

Each column of the response matrix d_{ij} contains information about the response of edge velocity to a single node displacement. One such response is demonstrated in Fig. 7.3.

As can be seen, neighboring nodes of the node j with surface jump $\Delta\delta^*_j$ are subject to drop in edge velocity of about half the magnitude of the velocity growth at j-th node. This can be also observed by comparing the values of subdiagonal and superdiagonal with main diagonal of the response matrix.

Based on these observations, new replacement inviscid model has been formulated which can be used for boundary edge velocity updates between boundary layer passes:

$$u_{e\,i} = u_{e\,i,orig} + d_{ii}(\delta^*_i - 0.5\delta^*_{i-1} - 0.5\delta^*_{i+1}) \tag{7.6}$$

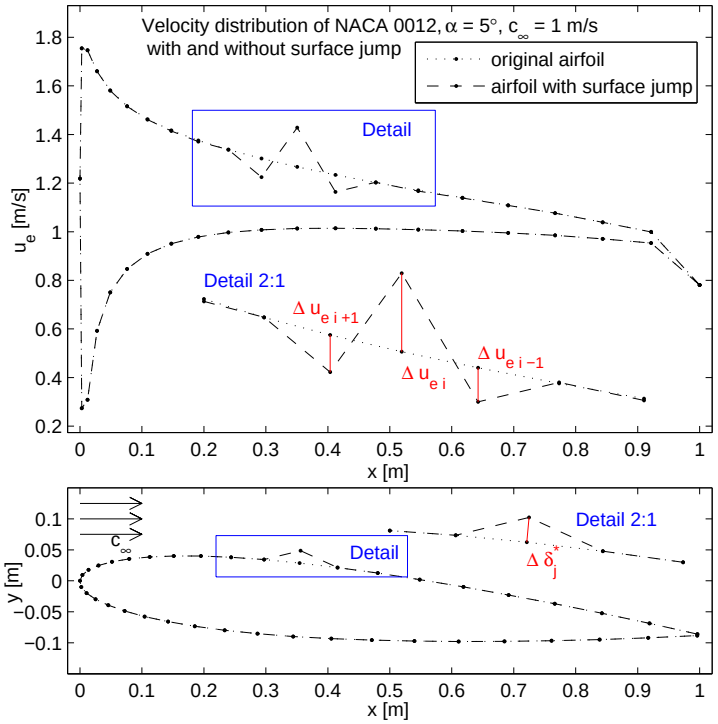

FIGURE 7.3: Response of velocity to surface jump. Note: Surface displacement has been exaggerated for illustration purposes

When the replacement inviscid model is used together with the boundary layer model, the only input parameters needed are the velocity distribution with surface coordinates. This makes the resulting boundary layer truly portable with small impact on results accuracy. In order to connect the boundary layer to the 3D panel method, streamlines must be identified on the surface of the body. Example of such streamlines is in Fig. 7.4.

The model composed of 3D panel method with boundary layer has been tested using case of finite wing and results were compared against CFD RANS solver in [A 5].

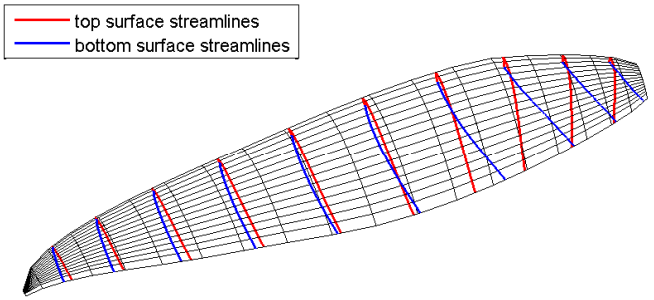

FIGURE 7.4: Surface streamlines of a heavily loaded propeller blade.

8. Experimental Investigation of Contra-Rotating Propellers

The experimental setup used for measurement of contra-rotating propellers is composed of a four-component aerodynamic scale, pair of coaxial electric motors and a support frame which also holds protective mesh and acoustic insulation. The aerodynamic scale is built around Double Axi 5330/20 coaxial motors and measures torque and thrust of each propeller. In addition to measuring thrusts and torques, rpm of each propeller is measured using optical means. The motors can provide up to 3kW of power each, which is sufficient for propeller sizes up to 24" (609.6 mm) in diameter. The mechanical design of the test stand allows limited modification of propeller distance in the range of 40 mm to 80 mm. Speed of rotation is controlled by a PWM signal and power is supplied by 24V lead-acid battery. Signal from load cells is sampled and analyzed by a custom built 12 channel A/D converter. An automatic measurement cycle is started and monitored using a graphical user interface scripted in MATLAB. The experimental setup and results from measurement are described in detail in a conference paper [A 6] by the author et al.

A supplementary measurement of noise in terms of overall sound pressure level and sound spectra was performed. Details of noise measurement setup are in [A 6].

Aero-elastic properties of small scale aircraft propellers were obtained by analyzing the shape of the rotating blades photographed by a camera and a flash synchronized to the blade position. Detailed description and results can be found in [A 7]. The research revealed that bending of the blades forward occurs with increasing thrust. This bending is reduced by centrifugal forces, which prevents the blades from bending even further under higher rpms. No detectable blade twist was observed.

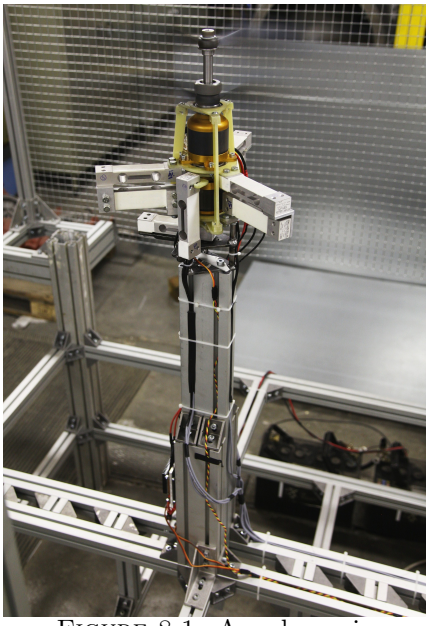

FIGURE 8.1: Aerodynamic balances mounted on a rigid support column.

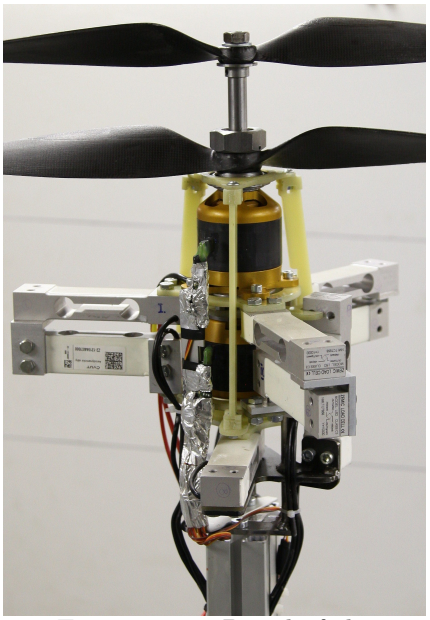

FIGURE 8.2: Detail of the aerodynamic balances.

9. Results, Analysis and Discussion

9.1 Verification of the models

Data from the measurement of an APC 20 × 13 [A 8] propeller were selected for verification of the numerical model in a single propeller test scenario. The calculated and experimental performance curves are shown in Fig. 9.1. Based on the results, 3D panel method with boundary layer matches experimental data more accurately for all advance ratios above 0.1, while near static thrust, lifting line solution coincides with experiment more accurately.

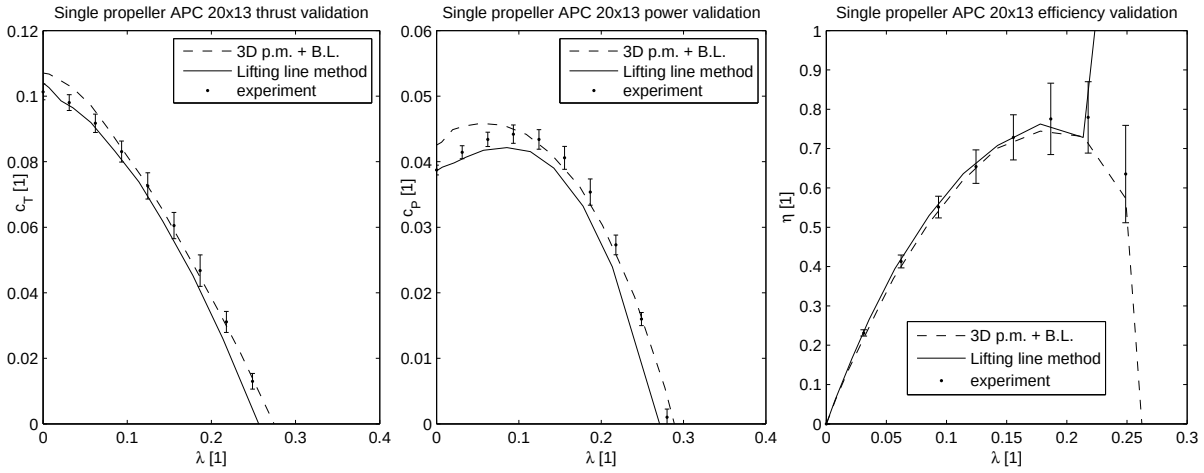

FIGURE 9.1: Comparison of lifting line model results with experiment and 3D panel method with boundary layer. Case of a single propeller APC 20 × 13.

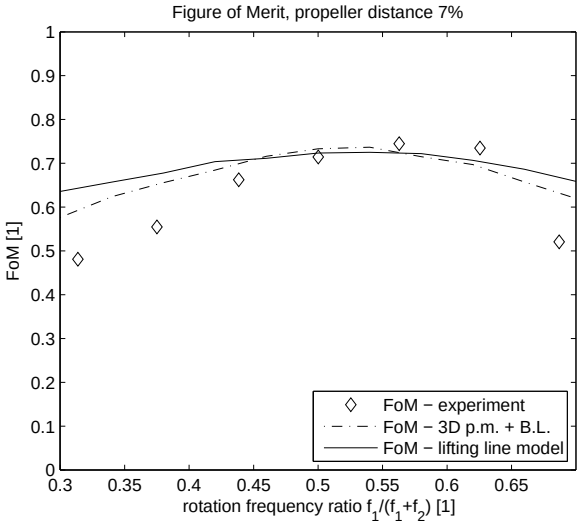

FIGURE 9.2: Figure of Merit vs. ratio of frequency of rotation.

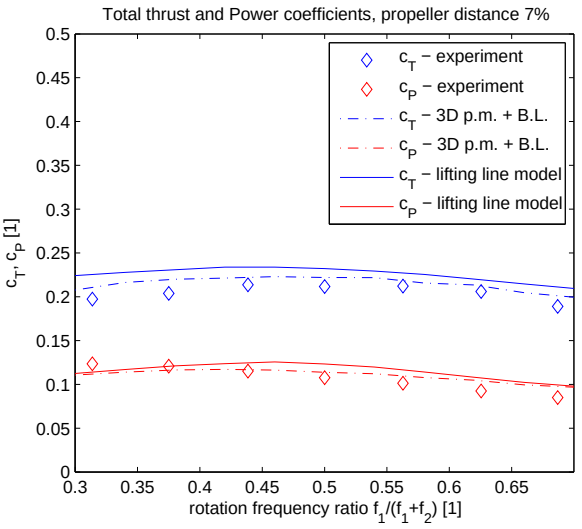

FIGURE 9.3: Total thrust and power coefficients of the system vs. ratio of frequency of rotation.

Effects of variable rotational rate ratio defined as $f_1/(f_1 + f_2)$ was studied on a CRP set of 22" propellers under static conditions. The results in terms of FoM and overall thrust

and power coefficients are shown in Figs. 9.2 and 9.3. Here the benefit of using 3D panel method is clearly visible. The results of verification were published in [A 9].

9.2 Results of numerical analysis of CRP

The computational model based on 3D panel method with boundary layer allows fast analysis of cases and conditions which would be difficult to investigate experimentally. An example of calculated unsteady forces during several rotations of the CRP propellers is in Fig. 9.4 Such results could not be easily measured, due to dynamic properties of the measurement system.

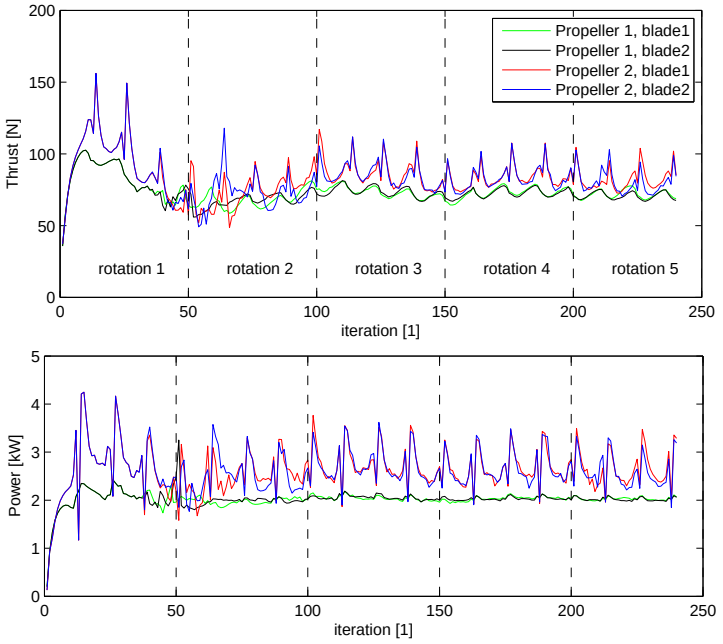

FIGURE 9.4: Unsteady values of thrust and power during initial 5 rotations.

Thanks to the force-free wake model described in Chapter 5, wake shapes can be visualized and studied, such as those in Fig. 9.5 illustrating the effect of advance ration.

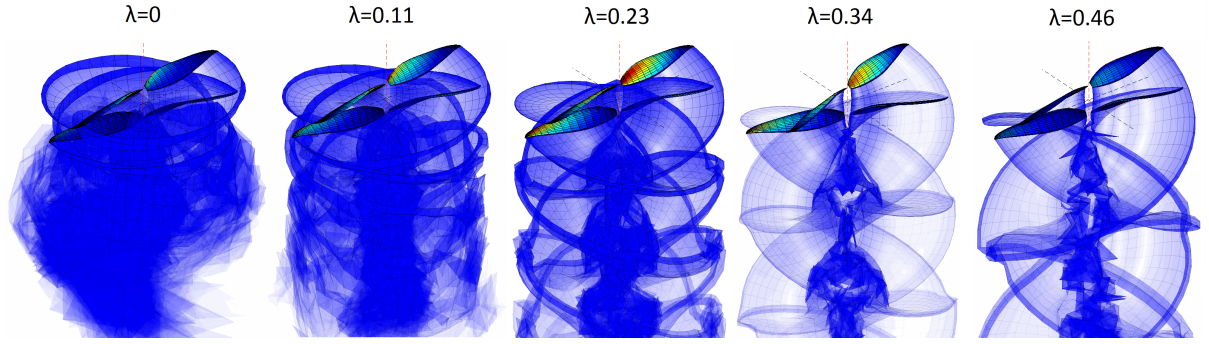

FIGURE 9.5: Development of CRP wakes for selected advance ratios.

Sensitivity of CRP system to propeller distance is relatively low, Figure of Merit slightly increases with propeller distance due to additional air being sucked in between the rotors (Fig. 9.6). The thrust is redistributed as shown in Fig. 9.7

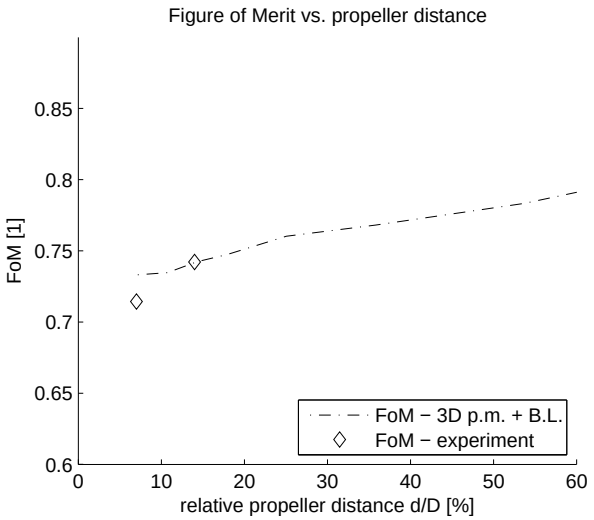

FIGURE 9.6: Figure of Merit vs. propeller distance.

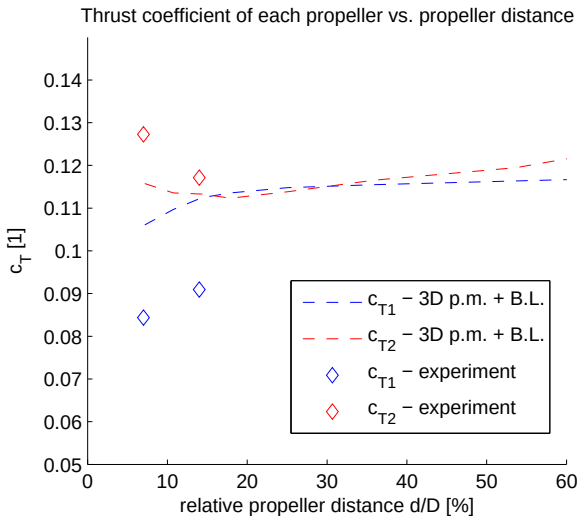

FIGURE 9.7: Thrust coefficient of each propeller vs. propeller distance.

When compared to an equivalent single propeller, CRP provides up to 6% increase in efficiency (Fig. 9.8). The comparison needs to be performed at the same thrust levels, because efficiency is very sensitive to loading of the propeller. Largest increase in efficiency occurs for low advance ratios, where swirl losses play an important role.

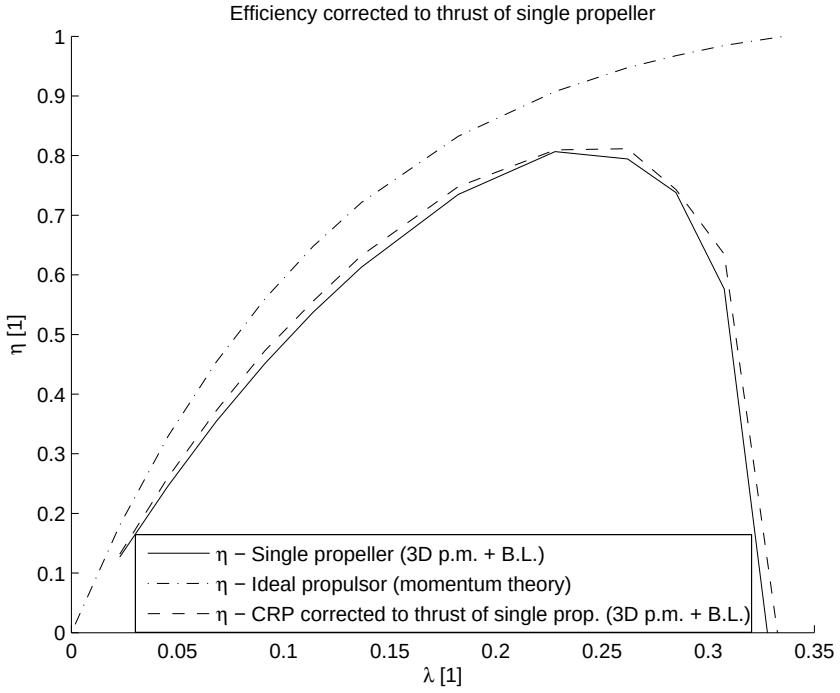

FIGURE 9.8: Efficiency of propulsion systems at the same thrust vs. advance ratio.

A CRP system, when subjected to off-axis free stream, shows little sensitivity to small inflow angles while for increasing angles the performance benefits from additional lift due to forward flight. This is a typical scenario where simpler computational methods using various simplifications cannot be used, because the flow is not axisymmetric.

10. Conclusions and Recommendations

A 2D boundary layer was successfully coupled to a 3D panel method using a new viscous-inviscid interaction model thus extending the capabilities of the originally inviscid model. The results of verification indicate that 3D panel method with boundary layer is more accurate than lifting line approach especially in the case of CRP analysis. On the other hand, inviscid 3D panel method falls short of the performance of simpler lifting line model due to absent viscous effects, which cause overprediction of thrust and efficiency. Both blade representation models benefit from the unsteady force-free wake model. Inclusion of a vortex core model with core radius growth contributed to the stability of the solution by removing singularity problems.

A CRP system has been analyzed with some of the numerical model results also supported by experimental work. Performance under off-design conditions such as extreme propeller rotational rate ratios or off-axis inflow angles were studied. Partially stalled blades and wake development under static thrust conditions were among the demanding circumstances that the numerical method was set to cope with.

10.1 Contribution in the field of computational methods

The main contribution to the field of computational methods is the description of new effective viscous-inviscid interaction between inviscid solver and boundary layer model and practical demonstration of the implementation to contra-rotating propellers. Another contribution is the force-free wake model, which includes vortex stretching and aging, and which allows mutual intersection of wakes and blade passage. Many minor problems had to be solved along the way. Lifting line model tip treatment, propeller wake blow-off method and various improvements in the speed of solution are also considered as practical contributions.

10.2 Contribution in the field of propeller aerodynamics

The following conclusions about the performance of CRP systems were reached:

- Response of a contra-rotating propeller system to change of ratio of frequencies of rotation showed that peak Figure of Merit is obtained for slightly different propeller rotational frequency ratio than 1:1. Although the most effective ratio depends on the exact geometry and conditions, it can be generalized that by controlling the ratio of rotation of propellers throughout the operation range, overall efficiency can be increased.

- Increasing propeller distance redistributes thrusts and slightly increases the values of Figure of Merit, while reducing noise. Propellers should be placed as far apart as possible and practical.

- Performance of a CRP system is initially insensitive to angle of off-axis free-stream velocity, only at angle higher than 30° the efficiency begins rising due to the effect of additional lift provided by forward flight component of velocity.

- CRP system and equivalent single propeller of the same diameter and blade solidity must be compared strictly at the same thrust level, otherwise incorrect conclusions may be

drawn. At the same thrust levels, contra-rotating propeller system provides $1 \div 6\%$ increase in efficiency over equivalent single propeller. The increase is more evident for low advance ratios, where the propellers are more loaded.

- Both upstream and downstream propellers are subject to fluctuating thrust force. The upstream propeller experiences rather smooth and gradual changes of thrust, while the downstream propeller is subject to sharp peaks in thrust when the blades pass through wakes. Power of the upstream propeller is almost constant in time, while the power of downstream propeller suffers peaks corresponding to thrust oscillations.

10.3 Recommendations on the future work

The presented numerical model can be used "as is" for various other tasks including wind turbine analysis or UAV flight simulation. It is very suitable for optimization problems where CFD solvers cannot possibly compete due to time of solution. Parameters such as propeller geometry or rotational rate ratio can be optimized for maximum efficiency.

Minor improvements to the model in terms of speed and accuracy can be made. Simplification of wake far downstream from propellers or removing re-inicialization of boundary layer between time steps are among suggested improvements.

Extending the capabilities of the model is also an option. Compressibility effects can be accounted for by simple corrections such as Prandtl-Glauert or Kármán-Tsien compressibility corrections. Some features, such as ducts and hubs, could be simulated using panels or circular vortex rings. After such modification, it would be possible to analyse ventilation fans, ducted fans, configurations with stator blades and similar cases.

References

[1] Wald, Q. R. (2006). The aerodynamics of propellers. *Progress in Aerospace Sciences*, vol. 42, pp. 85–128. ISSN 0376-0421.

[2] Leishman, J. G. and Ananthan, S. (2006). Aerodynamic optimization of a coaxial proprotor. In: *62nd American Helicopter Society International Annual Forum*. p. 64.

[3] Rand, O. and Khromov, V. (2010). Aerodynamic optimization of a coaxial rotor in hover and axial flight. In: *27th International Congress of the Aeronautical Sciences*. IACS, pp. 1–13.

[4] Yang, C., Tamashima, M., Wang, G. Q., Yamazaki, R. and Koizuka, H. (1992). Prediction of the unsteady performance of contra-rotating propellers by lifting surface theory. *Transactions of the West-Japan Society of Naval Architects*, vol. 83, pp. 17–31.

[5] Hess, J. L. and Valarezo, W. O. (1985). Calculation of steady flow about propellers using a surface panel method. *Journal of Propulsion and Power*, vol. 1(6), pp. 470–476. ISSN 0748-4658.

[6] Hsin, C. (1990). *Development and Analysis of Panel Methods for Propellers in Unsteady Flow*. Ph.D. thesis, Massachusetts Institute of Technology.

[7] Ghassemi, H. (2009). Hydrodynamic performance of coaxial contra-rotating propeller (ccrp) for large ships. *Polish Maritime Research*, vol. 59(1), pp. 22–28. ISSN 1233-2585.

[8] Takinaci, A. C. and Atlar, M. (2001). On the importance of boundary layer calculations instead of viscous correction in heavily loaded marine propellers while using a surface panel method. *Ocean Engineering*, vol. 28, pp. 519–536. ISSN 0029-8018.

[9] Brizzolara, S., Villa, D. and Gaggero, S. (2008). A systematic comparison between RANS and panel methods for propeller analysis. In: *8th International Conference on Hydrodynamics*. pp. 1–13.

[10] Kim, H. W. and Brown, R. E. (2010). A comparison of coaxial and conventional rotor performance. *Journal of the American Helicopter Society*, vol. 55(1), pp. 12004–12004. ISSN 0002-8711.

[11] Heyong, X. and Zhengyin, Y. (2011). Numerical simulation of unsteady flow around forward flight helicopter with coaxial rotors. *Chinese Journal of Aeronautics*, vol. 24(1), pp. 1–7. ISSN 1000-9361.

[12] Paik, K., Hwang, S., Jung, J., Lee, T., Lee, Y., Ahn, H. and Van, S. (2015). Investigation on the wake evolution of contra rotating propeller using RANS computation and SPIV measurement. *International Journal of Naval Architecture and Ocean Engineering*, vol. 7(3), pp. 595–609. ISSN 2092-6782.

[13] Harrington, R. D. (1951). Full-scale-tunnel investigation of the static-thrust performance of a coaxial helicopter rotor. Tech. Rep. 2318, NASA.

[14] Dingeldein, R. C. (1954). Wind-tunnel studies of the performance of multirotor configurations. Tech. Rep. 3236, NASA.

[15] Coleman, C. P. (1997). A survey of theoretical and experimental coaxial rotor aerodynamic research. Tech. Rep. 3675, NASA.

[16] Huo, C., Barenes, R. and Gressier, J. (2015). Experimental analysis of the aerodynamics of long-shrouded contrarotating rotor in hover. *Journal of AHS*, vol. 60(4), pp. 1–12. ISSN 0002-8711.

[17] Simoes, C. (undated). Optimizing a coaxial propulsion system to a quadcopter. Tech. rep., Instituto Superior Tecnico.

[18] Ramasamy, M. (2013). Measurements comparing hover performance of single, coaxial, tandem and tilt-rotor configurations. In: *AHS 69th Annual Forum*. pp. 1–23.

[19] Katz, J. and Plotkin, A. (2001). *Low-Speed Aerodynamics*. Cambridge Aerospace Series, Cambridge University Press. ISBN 9780521665520.

[20] Drela, M. (1989). XFOIL – An analysis and design system for low Reynolds number airfoils. *Low Reynolds number aerodynamics*.

[21] Smith, A. and Hess, J. (1962). Calculation of non-lifting potential flow about arbitrary three-dimensional bodies. Tech. Rep. E.S. 40622, Douglas Aircraft Company, Inc., Long Beach, CA.

[22] Hess, J. (1972). Calculation of potential flow about arbitrary three dimensional lifting bodies. Tech. Rep. MDC J5679-01, McDonnell Douglas Corporation, Long Beach, CA.

[23] Morino, L. and Kuot, C. (1974). Subsonic potential aerodynamics for complex configurations: A general theory. *AIAA Journal*, vol. 12, pp. 191–197. ISSN 0001-1452.

[24] Erickson, L. (1990). Panel methods - an introduction. Tech. Rep. Technical Paper 2995, NASA, Ames Research Center, Moffet Field, CA.

[25] Lamb, H. (1916). *Hydrodynamics, Fourth edition*. London: Cambridge University Press.

[26] Burnham, D. C. and Hallock, J. N. (1982). Chicago monostatic acoustic vortex sensing system. Tech. Rep. DOT-TSC-FAA-79-104.IV, Transportation Systems Center Cambridge MA.

[27] Vatistas, G. H., Kozel, V. and Mih, W. C. (1991). A simpler model for concentrated vortices. *Experiments in Fluids*, vol. 11, pp. 73–76. ISSN 0723-4864.

[28] Batchelor, G. K. (1967). *Introduction to Fluid Dynamics*. Cambridge University Press. ISBN 0521663962.

[29] Saffman, P. G. (1992). *Vortex Dynamics*. Cambridge Monographs on Mechanics, Cambridge University Press. ISBN 978-0521477390.

[30] Anathan, S. and Leishman, J. (2004). Role of filament strain in the free-vortex modeling of rotor wakes. *Journal of the American Helicopter Society*, vol. 49(2), pp. 176–191. ISSN 0002-8711.

[31] Drela, M. . and Giles, M. (1987). Viscous-inviscid analysis of transonic and low Reynolds number airfoils. *AIAA Journal*, vol. 25(10), pp. 1347–1355. ISSN 0001-1452.

[32] Johansen, J. (1997). *Prediction of laminar/turbulent transition in airfoil flows*. Roskilde: Risø National Laboratory. ISBN 87-550-2308-8.

[33] Green, J. E., Weeks, D. and Brooman, J. (1977). Prediction of turbulent boundary layers and wakes in compressible flow by a lag-entrainment method. *NASA STI/Recon Technical Report N*, vol. 77.

[34] Veldman, A. E. P. (1981). New, quasi-simultaneous method to calculate interacting boundary layers. *AIAA Journal*, vol. 19(1), pp. 79–85. ISSN 0001-1452.

[35] Bijleveld, H. and Veldman, A. E. P. (2013). Prediction of unsteady flow over airfoils using a quasi-simultaneous interaction method. Tech. rep., ECN Wind Energy.

[36] Goldstein, S. (1948). On laminar boundary-layer flow near a position of separation. *The Quarterly Journal of Mechanics and Applied Mathematics*, vol. 1(1), pp. 43–69.

[37] Veldman, A. E. P. (2009). A simple interaction law for viscous–inviscid interaction. *Journal of Engineering Mathematics*, vol. 65(4), pp. 367–383. ISSN 0022-0833.

Cited work of the author

[A1] Štorch, V. and Nožička, J. (2016). A novel computational model for the analysis of contra-rotating propellers. In: *Fluid Mechanics and Thermodynamics, Proceedings of Students' Work in the Year 2015/2016*. Prague: Czech Technical University in Prague, Faculty of Mechanical Engineering, pp. 95–105. ISBN 978-80-86786-38-4.

[A2] Štorch, V., Nožička, J., Brada, M. and Suchý, J. (2015). Experimental verification of computational model for wind turbine blade geometry design. In: *Experimental Fluid Mechanics 2014*. Český Krumlov: Technical University of Liberec, vol. 92 of *EJP Web of Conferences*, pp. 1–6. ISSN 2101-6275.

[A3] Štorch, V. and Nožička, J. (2014). 3D panel methods for turbomachinery design. In: *Fluid Mechanics and Thermodynamics, Proceedings of Students' Work in the Year 2013/2014*. Prague: Czech Technical University in Prague, Faculty of Mechanical Engineering, pp. 43–51. ISBN 978-80-86786-36-0.

[A4] Štorch, V. and Nožička, J. (2015). On viscous-inviscid interaction for boundary layer calculation using two-equation integral method. In: *Fluid Mechanics and Thermodynamics, Proceedings of Students' Work in the Year 2014/2015*. Prague: Czech Technical University in Prague, Faculty of Mechanical Engineering, pp. 81–97. ISBN 978-80-86786-37-7.

[A5] Štorch, V. and Nožička, J. (2017). Verification and possible applications of new 3D panel method with boundary layer. In: *Fluid Mechanics and Thermodynamics, Proceedings of Students' Work in the Year 2016/2017*. Prague: Czech Technical University in Prague, Faculty of Mechanical Engineering, pp. 29–46. ISBN 978-80-86786-39-1.

[A6] Štorch, V., Nožička, J. and Brada, M. (2017). Experimental setup for measurement of contra-rotating propellers. In: *Topical Problems of Fluid Mechanics 2017*. Prague: Institute of Thermomechanics ASCR, pp. 285–294. ISSN 2336-5781.

[A7] Štorch, V., Nožička, J., Brada, M. and Suchý, J. (2016). Measurement of noise and its correlation to performance and geometry of small aircraft propellers. In: *Experimental Fluid Mechanics 2015*. vol. 116 of *EPJ Web of Conferences*, pp. 1–6. ISSN 2100-014X.

[A8] Filipský, J. and Štorch, V. (2014). Comparison of propeller analysis methods and experimental data. In: *Engineering Mechanics 2014*. Brno University of Technology, pp. 172–175. ISSN 1805-8248.

[A9] Štorch, V. and Nožička, J. (2017). Contra-rotating propeller aerodynamics solved by a 3D panel method with coupled boundary layer. *Acta Polytechnica*, vol. 57(5), pp. 355–366. ISSN 1210-2709.

Other work of the author

Conference papers in proceedings:

[i] Štorch, V. (2015). Dmychadlem poháněný UL letoun se záporným úhlem šípu křídla a s kachní vodorovnou ocasní plochou. In *KSMTaT 2015*, Litoměřice, FVTM UJEP.

[ii] Čížek, J., Dvořák, L., Filipský, J., Sumara, Z., Štorch, V., Vitkovič, P and Vitkovičová, R. (2015). Oblasti výzkumu aktuálně řešené na ÚMTaT In: *29th Symposium on Anemometry*. Praha: Institute of Hydrodynamics ASCR, pp. 5-8. ISBN 978-80-87117-13-2.

[iii] Vitkovič, P., Štorch, V., Punčochář, J. and Stodůlka, J. (2016). Measurement of thermal performance of hybrid cooling tower In: *Proceedings of the 35th Meeting of Departments of Fluid Mechanics and Thermomechanics*. New York: AIP Conference Proceedings. ISBN 978-0-7354-1426-6.

Technical reports:

[i] Hyhlík, T., Čížek, J., Filipský, J., Štorch, V., Sumara, Z., Borovička, M., Devera, J., Kalinay, R. et al. (2016). Cooperation on Several Topics such as Tumble Dryers, High Speed Fan and Dishwashers 2016, Porcia, Pordenone: Electrolux Italia SpA, GTC - Global Technology Center. Z-ELX-1/16.

[ii] Štorch, V. (2016) Rozložení teplot na povrchu výstelky vzduchovodu letounu L-59 při napojení na zařízení PARNO 2016.

[iii] Štorch, V. and Čížek, J. (2015). SW pro návrh a analýzu systémů pneumatické dopravy, Beumer.

[iv] Filipský, J., Čížek, J., Kantor, M., Štorch, V., Nožička, J., Javorek, T., Sklenář, P. and Štěch, S. (2014). Analýza měřicích řetězců.

[v] Štorch, V., Čížek, J. and Nožička, J. (2014). Trať pro měření tlakové ztráty elektromotorů. SEL-2014-1.

[vi] Štorch, V., Čížek, J. and Nožička, J. (2014) Optimalizace tvaru profilu lopatky ve 2D a 3D potenciálním proudění za použití panelových metod. MAV-2014-1.

[vii] Čížek, J., Štorch, V. and Nožička, J. (2013) Optimalizace tvaru lopatky pro Francisovy a kaplanovy vodní turbíny. SV-2013/2.